Structure of an integrin αIIbβ3 transmembrane-cytoplasmic heterocomplex provides insight into integrin activation

Jun Yang, Yan-Qing Ma, Richard C. Page, Saurav Misra, Edward F. Plow, and Jun Qin[1]

Department of Molecular Cardiology NB20, Lerner Research Institute, Cleveland Clinic, 9500 Euclid Avenue, Cleveland, OH 44195

Communicated by Angela M. Gronenborn, University of Pittsburgh, Pittsburgh, PA, August 24, 2009 (received for review July 29, 2009)

Heterodimeric integrin adhesion receptors regulate diverse biological processes including angiogenesis, thrombosis and wound healing. The transmembrane-cytoplasmic domains (TMCDs) of integrins play a critical role in controlling activation of these receptors via an inside-out signaling mechanism, but the precise structural basis remains elusive. Here, we present the solution structure of integrin αIIbβ3 TMCD heterodimer, which reveals a right-handed coiled-coil conformation with 2 helices intertwined throughout the transmembrane region. The helices extend into the cytoplasm and form a clasp that differs significantly from a recently published αIIbβ3 TMCD structure. We show that while a point mutation in the clasp interface modestly activates αIIbβ3, additional mutations in the transmembrane interface have a synergistic effect, leading to extensive integrin activation. Detailed analyses and structural comparison with previous studies suggest that extensive integrin activation is a highly concerted conformational transition process, which involves transmembrane coiled-coil unwinding that is triggered by the membrane-mediated alteration and disengagement of the membrane-proximal clasp. Our results provide atomic insight into a type I transmembrane receptor heterocomplex and the mechanism of integrin inside-out transmembrane signaling.

NMR | protein structure | transmembrane domain

Integrins are a major class of cell adhesion receptors that are found in almost every living organism (1). They are obligate heterodimers (α,β) in which each subunit is composed of a large extracellular domain, a single pass transmembrane (TM) segment, and a small cytoplasmic tail (CT). Integrins interact with extracellular matrix (ECM) proteins via their extracellular domains and with intracellular proteins via their CTs. This interconnection allows integrins to regulate diverse cellular adhesive processes. A central and unresolved issue in integrin biology is the molecular basis for signal transmission across the cell membrane. A large body of genetic, cell biological, and biochemical data indicate that the conformational states of integrin α/β transmembrane-cytoplasmic domains (TMCDs) control the ability of integrins to bind extracellular ligands (inside-out signaling) and to cluster and form focal adhesions (outside-in signaling) (for reviews see refs. 1 and 2). Biochemical and structural evidence suggests that the α/β TMCDs associate via both their TMs (3–6) and their CTs (7–9) to maintain integrins in a resting state. Dissociation of the TMs or CTs triggers receptor activation and signaling (7, 10–14). However, many different computational models for the TM association exist (3–5, 11, 13, 15–18) and the structural analyses of the CT interaction are inconsistent (6–9, 19). Earlier studies failed to observe heterodimeric TMCD interaction in micelles (20), which reflects the technical difficulty in structurally characterizing this kind of transmembrane heterodimers (21). Here, we have successfully determined the NMR structure of the αIIbβ3 TMCD heterodimer encompassing complete αIIbβ3 TMCD sequences. During the preparation of our manuscript, Lau et al (6) reported the structure of the αIIbβ3 TM heterodimer containing TMs and truncated portion of the CTs. Our structure agrees with Lau et al (6) on the TM assembly but differs significantly on the CT portion—the center for communicating signals across the membrane (1, 2). Further functional analysis and detailed structural comparison suggest a concerted conformational transition process that may be responsible for triggering the potent integrin αIIbβ3 activation. Since the TMCDs are highly conserved across integrins (1), our analyses may also shed light on the general mechanisms of transmembrane signaling in integrins.

Results and Discussion

Structure Determination of the αIIbβ3 TMCD Complex. Structural determination of heterodimeric TM complexes is challenging due to their highly dynamic nature (21). Since NMR is a unique tool to study weak/dynamic complexes, we decided to pursue the NMR structure of the αIIbβ3 TMCD complex. A series of isotope-labeled and unlabeled αIIb TMCD (residues E^{960}-E^{1008}) and β3 TMCD (residues K^{689}-T^{762}) constructs, each encompassing the entire TM segment and CT, were prepared. The recent crystal structure of the αIIbβ3 ectodomains (22) ends at αIIb A^{958}/β3 G^{690} and hence our constructs essentially complete the remainder of the integrin C-terminal portions. A variety of membrane-mimetic solvents, including detergent micelles, bicelles, and organic compound/water mixtures, were explored to optimize detection of the αIIb/β3 TMCD interactions. Of all of the conditions tested, the CD_3CN/H_2O (1:1) mixture yielded the highest quality NMR spectra and showed evidence of site-specific αIIb/β3 TMCD interaction (Fig. S1 *A* and *B*. The detailed description and justification of sample conditions are also provided in the *SI Method*). The sites of interaction between the subunits are localized in the TM and membrane-proximal CTs (Fig. S1 *A* and *B*), demonstrating the specific αIIb/β3 TMCD heterodimerization, consistent with results in mammalian cell membranes (14). The interaction is modest as judged by the extent of chemical shift changes but is consistent with the need for rapid and reversible TM signaling (21). Convincing intermolecular NOEs were obtained (Fig. S2), further demonstrating the specificity of the αIIb/β3 TMCD association and leading to a well-defined structure of the αIIbβ3 TMCD heterodimer (see details in Table S1).

Overall Structure of the αIIb/β3 TMCD Complex. Fig. 1 *A* and *B* illustrates the overall structure of the αIIb/β3 TMCD complex. In the complex, the αIIb TMCD displays α-helical features from I^{966} to N^{996} (31 residues) with 2 kinks, one around G^{976} (Fig. 1*C*) and the other around G^{991} (Fig. 1 *B* and *D*). The C terminus of αIIb (R^{997}-E^{1008}) is rich in acidic residues and largely unstruc-

Author contributions: J.Q. designed research; J.Y., Y.-Q.M., and R.C.P. performed research; J.Y., Y.-Q.M., R.C.P., S.M., E.F.P., and J.Q. analyzed data; and J.Y. and J.Q. wrote the paper.

The authors declare no conflict of interest.

Data deposition: The structure coordinates and other experimental parameters have been deposited to the Protein Data Bank, www.pdb.org (PDB ID code 2knc).

[1]To whom correspondence should be addressed. E-mail: qinj@ccf.org.

This article contains supporting information online at www.pnas.org/cgi/content/full/0909589106/DCSupplemental.

BIOCHEMISTRY

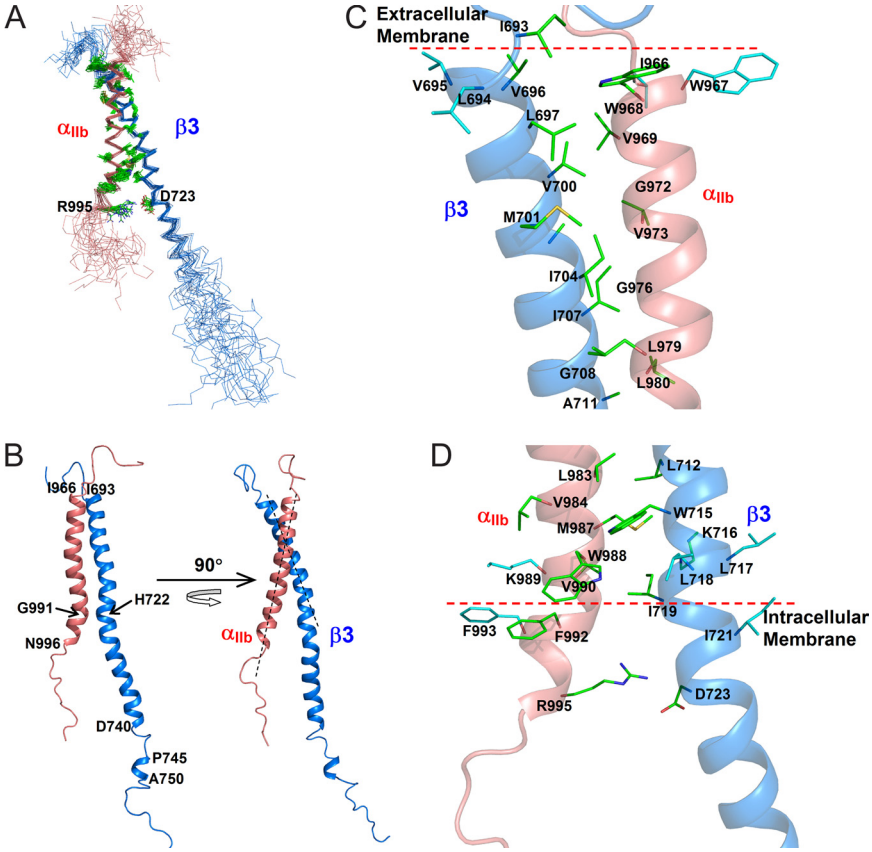

Fig. 1. Structure of integrin αIIbβ3 TMCD heterodimer. (*A*) Superposition of 20 calculated structures with the lowest energies showing how well the backbone and side chains of the interface containing regions are defined. Notably, the αIIb R995/β3 D723 side chains converge, pointing to each other at short distances and allowing salt bridge formation. (*B*) Two different views of the entire diagram of the αIIbβ3 TMCD heterodimer. Notice the significant kinks at the transmembrane-cytoplasmic border, which promote formation of the cytoplasmic clasp. (*C*) Detailed N-terminal half of the interface of the TMCD heterodimer. The side chains, not in the interface but involved in the extracellular membrane embedding, are also shown (colored in cyan). (*D*). Detailed C-terminal half of the interface. The side chains, not in the interface but involved in the membrane anchoring at the transmembrane-cytoplasmic border, are colored in cyan. The positions of the charged groups of αIIb K^{989} and β3 K^{716} (if linearly extended toward the membrane) indicate the TM-CT border (dotted line).

tured, as was observed previously (7, 23). The β3 TMCD has a much longer helix, I^{693}-A^{737} (45 residues) (Fig. 1*B*). The β3 helix curves in the TM region and contains one significant kink around H^{722}-D^{723} (Fig. 1*B*). Residues K^{738}-D^{740} also exhibit some helical features but the remaining sequence of residues, T^{741}-T^{762}, is largely extended except for a short helical turn (P^{745}-A^{750}) (Fig. 1*B*).

The detailed dimer interface is summarized in Fig. 1 *C* and *D*. At the extracellular membrane side, the interface begins with interactions of the αIIb W^{968} ring with β3 I^{693} and L^{697} (Fig. 1*C*). The bulky aromatic ring of αIIb W^{968} is positioned at the same spatial zone as the hydrophobic side chains of αIIb I^{966}/W^{967} and β3 L^{694}-V^{697} (Fig. 1*C*), suggesting that all these side chains are involved in extracellular membrane embedding/anchoring. The extracellular fragments in our construct (αIIb 960–965 and β3 689–692) exhibit short loop conformations and are spatially close, which match to the extensions of the associated C-terminal legs of the ectodomain in the crystal structure (22) (Fig. S3). This allows for the C-terminal legs of the ectodomain to tightly couple to the TM association near the extracellular membrane interface (Fig. S3). Following the αIIb W^{968}/β3 I^{693} and αIIb W^{968}/β3 L^{697} pairings is a sequential network of hydrophobic interactions that occur throughout the rest of the TM region (Fig. 1 *C* and *D*). Notable interactions involve the backbone of αIIb G^{972}/G^{976} with β3 V^{700}, M^{701}, and I^{704} side chains and the backbone of β3 G708 with the side chains of αIIb L^{979} and L^{980}, respectively (Fig. 1 *C* and *D*). The glycines at αIIb G^{972}/G^{976} and β3 G^{708} allow close interhelical packing in the N-terminal half of the TM and crossing of the αIIb and β3 TMCD helices at an approximately 30° angle (Fig. 1*B*). In contrast, the TM packing at the C-terminal half is primarily filled with extensive side chain-side chain interactions (Fig. 1*D*).

At the TM-CT border, the spatial positions of the positively charged groups of αIIb K^{989}/β3 K^{716} (Fig. 1*D*) suggest that they begin the cytoplasmic regions. However, it is possible that the side chains following membrane-proximal residues αIIb V^{990}-F^{993}, β3 L^{717}-I^{721} are inserted into or anchored onto the membrane (Fig. 1*D*), which may stabilize the relative orientations of the TM helices. The extent of the insertion of these residues may vary depending upon the functional/activation states of the receptor (6, 23–25). Consistent with previous structural characterization of the cytoplasmic αIIb/β3 complex (7), the TMCD complex also reveals an αIIb R^{995}/β3 D^{723} salt bridge (Fig. 1*D*). This salt bridge was indicated in the majority of our calculated structures, i.e., the αIIb R^{995} and β3 D^{723} point to each other (Fig. 1*A*). Functional studies have demonstrated the important role of this salt bridge in maintaining the receptor in the resting state (14, 26). Thus, its presence is strong evidence for the physiological relevance of our structure. Overall, the spatial contact between αIIb KVGFFKR and β3 KLLITIHD is consistent with a conserved membrane-proximal clasp in integrins (7, 9, 23).

Coiled-Coil Feature for the TM Interface. The intertwined helical packing in the TM interface has a distinct right-handed coiled-coil conformation (Fig. 1*B*). Careful examination of the interaction interface (Fig. 2*A*) reveals a supercoiling that can be characterized as an 11-residue hendecad repeat, a variation of the canonical 7-residue heptad repeat coiled coil (27). In such a repeat, there are 2 distinct position categories (Fig. 2*B*). At positions of index *a*/*h*, side chains of interfacial residues point toward the interhelical axis as "knobs." At positions of index *de*, side chains of interfacial residues face peripherally to form cavities—"holes." To compensate for *a*/*h*-indexed positions that may lead to intermolecular clashes, the residues in these positions usually adopt a "knobs-into-holes" configuration in which they pack against residues in *de* indices. This "knobs-into-holes" packing is observed in αIIbβ3 TM coiled coil, especially in the

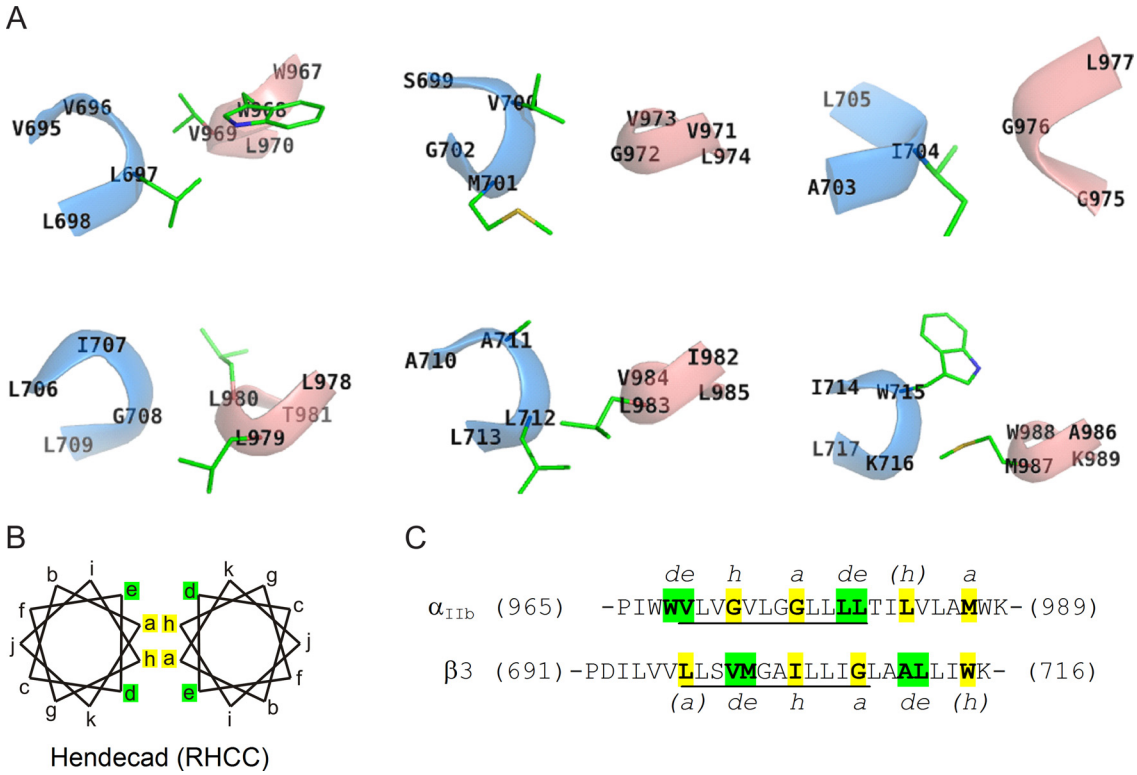

Fig. 2. Coiled coil features of αIIb/β3 TM interface. (*A*) Cross sections of each turn of both helices with the side-chains of interacting residues shown as sticks. The blue helix is β3 subunit and the red helix is αIIb subunit. (*B*) Helical wheel projections of a right-handed coiled coil with an 11-residue hendecad repeat (indexed *a*~*k*). (*C*) Sequences of the transmembrane domain of αIIb/β3. Residues occupying the *a*/*h* indices are colored yellow and *de* indices are colored green. The underlined regions show the most intensive intermolecular interactions and represent a classical hendecad repeat. The positions of residues with parenthesized indices are slightly shifted in the hendecad repeat extensions.

central region where extensive hydrophobic interactions are present (underlined regions in Fig. 2*C*).

The detailed interhelical interactions are as follows: in the central region, G^{972} in αIIb occupies the *h*-indexed position against V^{700}-M^{701} in β3 as indices *de*; G^{976} and I^{704} are indexed as *a* and *h* in αIIb and β3, respectively, and form a "knobs-into-knobs" interaction; and L^{979}-L^{980} in αIIb reside in *de*-indexed positions to accommodate residue G^{708}—the position of *a* in β3. The hendecad repeat extends to the N-terminal and C-terminal end of TM domain continuously. However, positions of residues assuming the *a*/*h* index in the extended regions are slightly shifted in the observed structure (Fig. 2 *A* and *C*), presumably due to the bulky tryptophan side chain nearby. For example, M^{987} in αIIb holds the *a* position and faces toward the interhelical axis as expected. However, the corresponding β3 residue W^{715} with index *h* points sideways instead of toward the interhelical axis as in a canonical hendecad repeat. The bulky indole group of tryptophan may necessitate such a position shift to avoid the steric clashes that would otherwise arise in this region. Similar arrangements may apply to the *a*/*h*-indexed L^{697} in β3 and L^{983} in αIIb. Such coiled-coil irregularities are quite common in proteins and often provide structural flexibilities that are important for functions (28, 29). The coiled-coil interface is highly conserved among integrins (Fig. S4) and may be a general feature of receptor heterocomplexes.

Correlation of the TMCD Interface with Integrin Mutation Data and Other Functional Data. The αIIbβ3 TMCD dimer structure provides a template to interpret the effects of previously reported point mutations on integrin activation. Table S2 lists all TMCD point mutations and their functional consequences. Notably, mutations which dramatically increase residue size in the closely packed helix crossing region, αIIb G^{972}L, G^{976}L, and β3 G^{708}L/I, should sterically clash at the interface, and these mutations uniformly lead to significant integrin activation. Other core interface mutations, including αIIb L^{980}A, L^{983}A, R^{995}A/D, β3 I^{704}A, I^{719}A/M, and D^{723}A/H, and disease mutations αIIb R^{995}Q and β3 D^{723}H would also impair heterodimerization and activate integrin (Table S2). Consistent with our structure, many noninterface mutations such as αIIb G^{975}L and β3 S^{699}L had little effect on integrin activation. Some interface edge (e.g., β3 A^{703}L) or conservative mutations (e.g., β3 M^{701}L) did not significantly activate the receptor presumably because of limited structural perturbations or minor interface adjustments (Table S2).

Great care needs to be taken when explaining the mutational data in the TM-CT border and other CT regions. Mutations in these regions may have multiple consequences such as disruption of heterodimerization, alteration of the TM membrane embedding or binding to potential cytoplasmic regulators. For example, αIIb F^{992}A or F^{993}A mutation was shown to activate αIIbβ3 (26). Based on our structure, F^{992}A may partially impair the clasp structure, and both F^{992}A and F^{993}A may impair the membrane anchoring of αIIb TM. However, both F^{992}A and F^{993}A were also shown to impair the binding of αIIb to CIB1 (30)—a negative regulator of the αIIbβ3 activation (31). Thus, F/A mutations may specifically activate αIIbβ3 through a combination of these effects. In contrast, the FF/AA mutation in the conserved GFFKR motif had little effect in the activation of another integrin, αVβ3 (32). These data suggest that there is differential regulation of the integrin activation by the TM-CT border, which may be due to the conformational complexity in this region. Another example, which is unrelated to the TMCD interface disruption, is provided by mutations in the membrane distal side of β3 CT. The E^{749}A mutation was found to activate αIIbβ3 (33) while the S^{752}P mutation inhibits receptor

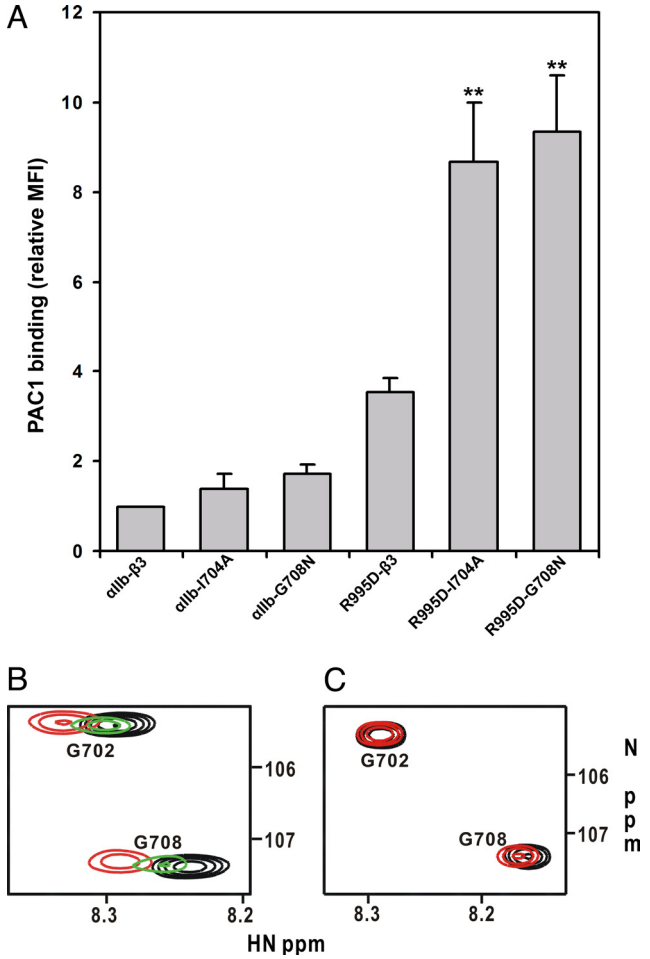

Fig. 3. Structural and functional effects of CT and TM mutations on integrin activation. (*A*) Quantitative comparison of the activation of wild type $\alpha_{IIb}\beta_3$ vs. mutants containing αIIb $R^{995}D$, β3 $I^{704}A$, β3 $G^{708}N$, and the double mutations αIIb $R^{995}D$/β3 $I^{704}A$ and αIIb $R^{995}D$/β3 $G^{708}N$. The extent of activation was determined from the ratio of PAC1 (activation specific mAb) to 2G12 (αIIbβ3 reactive mAb) binding as measured by FACS. This ratio was assigned a value of 1 for WT, and the activation state of each mutant is compared to WT (34). Results presented are means ± SD from 3 independent experiments. **, $P <$ 0.01 (vs. single mutation) by Student *t* test. (*B*) Representative regions of 2D ^{1}H-^{15}N HSQC spectra of 0.1 mM ^{15}N-labeled β3 TMCD in the absence (black) and presence of 0.3 mM WT αIIb TMCD (red) and 0.3 mM αIIb $R^{995}D$ mutant (green) showing that the mutation significantly weakens the αIIb/β3 TMCD association as judged by the substantially reduced chemical shift changes. (*C*) Representative regions of 2D ^{1}H-^{15}N HSQC spectra of 0.1 mM ^{15}N-labeled β3 TMCD $I^{704}A$ in the absence (black) and presence of 0.4 mM αIIb $R^{995}D$ (red) showing that mutations diminished the αIIb/β3 TMCD association since little chemical shift changes occur.

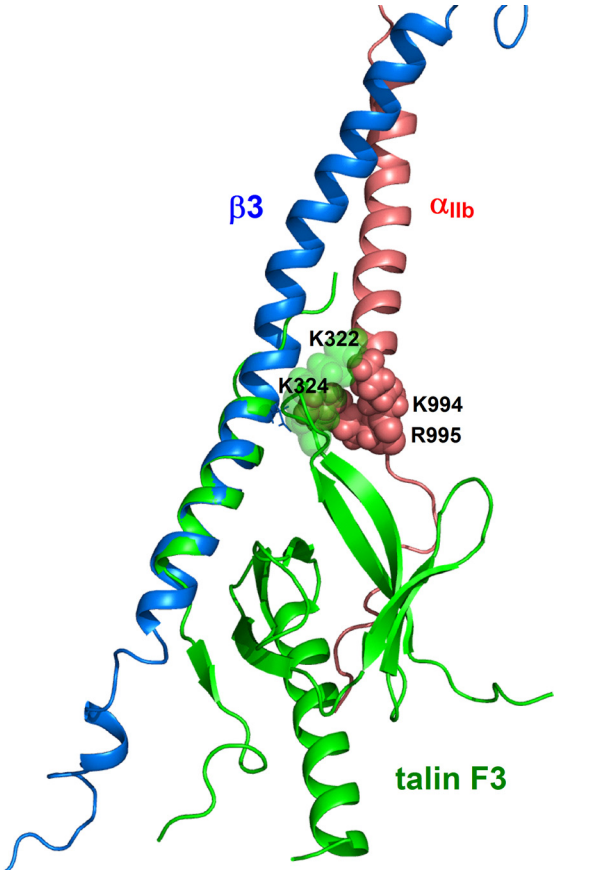

Fig. 4. Talin disrupts the CT clasp via steric clash and charge-charge repulsion. The β3 membrane-proximal region (bound to talin F3, PDB ID 2h7e) (H^{722}-A^{737}) (35) was superimposed with the same segment in the αIIbβ3 heterodimer, showing how talin F3 K322/K324 may directly interfere with αIIb K994/R995.

activation. These cannot be explained by TMCD interface disruption, and may be due to alterations in membrane-anchoring of the β3 distal CT (23) or binding to regulators.

To gain further insight into TMCD interface perturbation and integrin activation, we examined the extent of αIIbβ3 activation by mutations in the CT clasp and TM core interface (*a*) αIIb $R^{995}D$ and (*b*) β3 $I^{704}A$. While these mutations have been previously shown to activate the receptor (11, 14, 34), a systematic quantitative comparison of their individual effects and their combination has not been considered. Fig. 3*A* shows that αIIb $R^{995}D$ modestly activated the receptor and β3 $I^{704}A$ has a weaker effect. Remarkably, the combination of the 2 mutations exerted a strong synergistic effect, dramatically enhancing integrin activation (Fig. 3*A*). Similarly, another TM core interface mutation β3 $G^{708}N$ weakly activated the receptor but its combination with αIIb $R^{995}D$ had a synergistic effect (Fig. 3*A*). NMR binding experiments demonstrate that αIIb $R^{995}D$ substantially reduced the TMCD association (Fig. 3*B*) and its combination with β3 $I^{704}A$ abolished the interaction (Fig. 3*C*), demonstrating that both the TM and CT must dissociate to trigger potent integrin activation. The dissociation may be mediated by multiple factors, one of which involves talin (7, 10, 14, 35, 36). Fig. 4 shows the superposition of the β3 (H^{722}-A^{737}) bound to talin (35) with that in the αIIbβ3 TMCD complex. It provides a view of how talin may cause steric clash and charge-charge repulsion around the CT interface, therefore facilitating the TMCD dissociation.

Comparison with Other Integrin TM or CT Structures. As mentioned in the introduction, while our manuscript was in preparation, an NMR structure of the αIIb/β3 TM complex determined in bicelles was reported (6). Compared to our constructs that contain complete αIIb/β3 TM and CT sequences, the constructs in Lau et al. (6) lack most of the CT portions (αIIb truncated at P^{998} and β3 truncated at F^{727}). Comparison of the TM portions (αIIb L^{966}-W^{988}/β3 I^{693}-W^{715}) reveals that the 2 structures are very similar with an approximately 2.0 Å rmsd for the backbone (Fig. S5), indicating that both CD_3CN/H_2O mixture and bicelles provide environments compatible for TM complex assembly. Many different computational models of integrin TM complexes have been proposed (3–5, 11, 13, 15–18), but the 2 most recent ones (17, 18) were found to be similar to the structure of Lau et al. (ref. 6; discussed in detail in ref. 18). Thus, there is a general

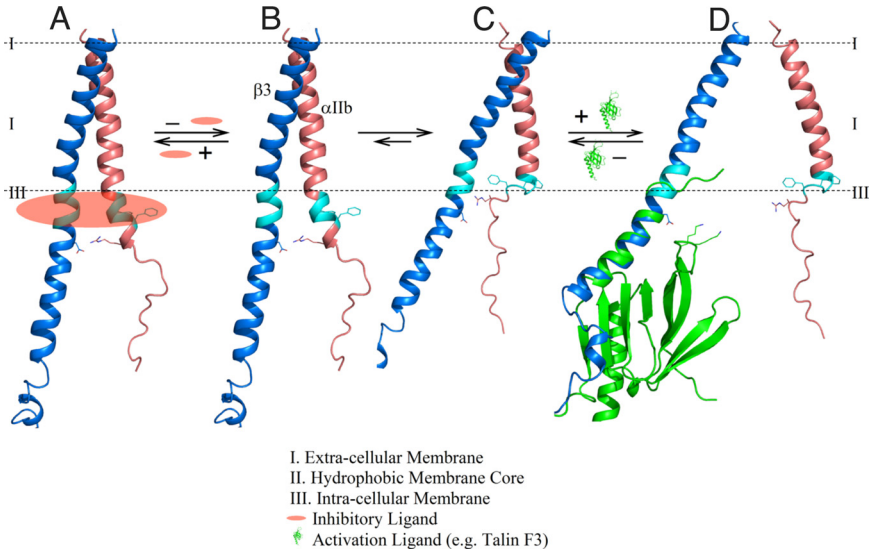

Fig. 5. A model for integrin inside-out TM signaling. (*A*). Step 1: the membrane-proximal clasp is bound to an inhibitor (shaded in red oval) that maintains the integrin at the resting state. (*B*). Step 2: a cellular signal dissociates the inhibitor from the clasp, leading to an intermediate state of the integrin TMCD heterodimer. (*C*). Step 3: the cytoplasm-exposed hydrophobic residues (in cyan) upon release of the inhibitor insert or anchors to the membrane, leading to the alteration and membrane-embedding of the clasp (in cyan). (*D*). Step 4: integrin regulators such as talin (in green) further perturb the clasp, leading to the dissociation of the clasp and subsequent unwinding of the TM coiled-coil. We note that talin could also compete with the inhibitor in Step 1 for binding to the clasp, but other regulators such as migfilin (40) may act synergistically to promote the release of the inhibitor more effectively.

agreement for integrin TM assembly from the latest independent studies (including ours) using different methods.

In the cytoplasmic region, the αIIb ^{989}KVGFFKR displays a helical conformation in our structure, in which αIIb ^{990}VGF weakly contacts β3 I^{719} and αIIb R^{995} forms a salt-bridge with β3 D^{723}. In contrast, in Lau et al. (6), the helix ends at αIIb V^{990} followed by an unusual left handed reverse turn (Fig. S5), which leads to the membrane-insertion and tight packing of the αIIb F^{992}/F^{993} aromatic rings with αIIb TM M^{987} and β3 TM L^{712}/I^{719} (6). Using a computational modeling program, membrane-Rosetta, Zhu et al. (17) also predicted a reverse turn conformation in the αIIb GFF region. To further examine this, we used a robust modification of Rosetta, CS-Rosetta (37), which includes the assigned backbone chemical shifts derived from the CD_3CN/H_2O medium as experimental constraints to better predict protein structure against the known protein structure database. The CS-Rosetta predicted the GFF reverse turn in the majority of the lowest energy conformations (Fig. S6), and only a small population of the low energy conformations had the GFF helical conformation (Fig. S6). This prediction is inconsistent with our NMR data that only detected the latter and no NOEs defining the reverse turn and the reverse turn-mediated clasp conformation were observed. Nevertheless, the CS-Rosetta data and the detection of the GFF reverse turn in bicelles (6) suggest that both conformations may exist and one or the other may predominate depending on the cellular environment. In this regard, we note that the intersubunit NOEs between the αIIb F^{992}/F^{993} aromatic rings and β3 L^{712}/I^{719} side chains, e.g., I^{719} CδH3 (see figure S4 in ref. 6), which are expected based on the reverse turn-mediated clasp conformation (6), were not observed, suggesting that such conformation is highly dynamic or transient. Since the TM packing is very similar between the 2 NMR structures (Fig. S5), the different CT clasps (Fig. S5) involving either the αIIb KVGFF reverse turn or helix cannot be due to the lack of TM as stated by Zhu et al. (17). Rather, different solvent systems (CD_3CN/H_2O vs. bicelles) in the 2 studies may have captured 2 different conformational states of an intrinsically flexible region. The overall topology of the CT clasp determined in CD_3CN/H_2O was found to be similar to the one determined in aqueous solution (Fig. S5) (7), suggesting that this clasp represents a native conformation in the aqueous cytoplasm. This cytoplasm-exposed clasp is physiologically important since it would allow the access to cytoplasmic binding proteins such as CIB1 (30) and filamin (38), both of which negatively regulate the integrin activation (31, 39, 40). The membrane-embedded clasp in Lau et al. (6) is clearly inaccessible to these cytoplasmic proteins and thus we propose that it may represent an intermediate state after dissociation from the cytoplasmic protein(s) during integrin activation.

Mechanism of Integrin Inside-Out Transmembrane Signaling. We have determined the structure of the integrin αIIbβ3 TMCD heterodimer encompassing the complete TM and CT sequences. Multiple lines of evidence indicate that our structure is physiologically relevant and provide significant insight into the mechanism of integrin activation: (*i*) the TM region is well-correlated with the extensive mutation data (Table S2); (*ii*) the CT region is similar to the previously determined CT clasp in aqueous solution (7) and it displays the functionally important αIIb R^{995}/β3 D^{723} salt bridge; (*iii*) the superposition of the CT region with the talin/β3 complex (35) shows how talin may sterically disrupt the CT clasp involving the salt bridge (Fig. 4), which explains the previous competition data (7, 23) and functional analyses (10, 14); (*iv*) the double TM/CT mutations based on our structure (Fig. 3*A*) correlate well with our NMR binding data (Fig. 3 *B* and *C*), demonstrating that both TM and CT have to dissociate to activate integrins (5, 6, 14).

A particularly unexpected finding in our study was that the CT clasp in our structure differs substantially from the one by Lau et al. (6) (Fig. S5). As indicated above, such difference is likely correlated with a regulatory pathway for the integrin inside-out signaling. We suggest that this pathway is not a simple CT unclasping/TM dissociation process as previously proposed (6). Rather, it involves a highly cooperative process containing multiple energy-driven conformational transition steps as highlighted in Fig. 5. In the resting state of the receptor (step 1), the clasp containing the αIIb KVGFF helix is exposed to the cytoplasm and accessible/bound to cytosolic regulators. Step 2 is an intermediate state but still resting state where negative regulators are dislodged by cellular triggers. Step 3 is another intermediate state where the clasp including αIIb KVGFF and β3 KLLITI is embedded into the membrane. This step is accompanied by a GFF helix-to-reverse turn transition and alteration of the TM helix embedding/tilting. The membrane-distal β3 CT may also undergo structural transition in this step, e.g., from β-strand bound to filamin (39) to α-helix anchored to the membrane surface (23). In final step 4, talin, which exposes its F3 domain upon activation (36), drives the CT unclasping and subsequent unwinding of the TM coiled-coil complex. These

steps are rapid, highly cooperative, and ultimately lead to potent receptor activation.

How does the TM coiled-coil unwinding effect couple to the juxtamembrane region of the integrin ectodomains? Previous EM and protein engineering experiments (41) indicated that the C-terminal legs of the integrin ectodomains splay apart during integrin ligation. Since the C-terminal legs of the ectodomain abut our structure of the TM interface via short and spatially close loops (Fig. S3), we can now understand at an atomic level how the C-terminal leg separation is tightly constrained by TM association. Clearly, TM coiled-coil unwinding releases a constraint on the ectodomains, allowing ligand-induced conformational changes, including the C-terminal leg separation, to take place. TM coiled-coil unwinding could further drive the disengagement of the extracellular legs of the ectodomains—a process that may occur in synchrony with ligand binding.

Experimental Procedures

Integrin αIIb/β3 Transmembrane-Cytoplasmic (TMCD) Domain Expression and Purification. The expression and purification of human integrin αIIb TMCD residues E^{960}-E^{1008} and the R^{995}D mutant, and β3 TMCD residues K^{689}-T^{762} and the I704A mutant are provided in *SI Methods*.

NMR Sample Preparation, Spectroscopy, and Structure Calculations. Initial sample condition screening was performed using 0.1 mM ^{15}N-labeled αIIb TMCD and 0.2 mM unlabeled β3 TMCD or vice versa. Vigorous efforts were made to explore the suitable sample condition for high resolution NMR studies (see details of NMR sample preparation in the *SI Method*); 50%/50% CD_3CN/H_2O gave excellent NMR spectra and allowed detailed structural characterization of specific interactions between the 2 subunits (Fig. S1).

Four sets of NMR samples were prepared for triple resonance NMR experiments in 50%/50% CD_3CN:H_2O: (*a*) 0.2 mM ^{15}N/^{13}C-labeled αIIb TMCD in the absence and presence of 0.6 mM unlabeled β3 TMCD; (*b*) 0.2 mM ^{15}N/^{13}C-labeled β3 TMCD in the absence and presence of 0.6 mM unlabeled αIIb TMCD; (*c*) 0.4 mM ^{15}N/100%^{2}H-labeled αIIb TMCD in the absence and presence of 1.2 mM unlabeled β3 TMCD; (*d*) 0.4 mM ^{15}N/100%^{2}H-labeled β3 TMCD in the absence and presence of 1.2 mM unlabeled αIIb TMCD. Detailed NMR experiments and structure determination procedures are provided in *SI Method*.

Site-Directed Mutagenesis, Transfection, and Integrin Activation Assay. The human cDNA of αIIb and β3 were cloned into the mammalian expression vector pcDNA3.1 (Invitrogen). The 3′ nucleotide sequences including the cytoplasmic tails of αIIb and β3 were subcloned into pBluescript II SK(+) Vector. Substitutions were introduced into αIIb and β3 using QuikChange Site-Directed Mutagenesis Kits (Stratagene). The nucleotide sequences of all mutants were confirmed. Different combinations of the αIIb and β3 cDNAs were cotransfected into CHO-K1 cells using lipofectamine™ 2000 (Invitrogen). The transfected cells were cultured for at least 24 h before further analyses. The activation of αIIbβ3 was measured using PAC1, a mAb specific for the active conformer of αIIbβ3 as described in ref. 34.

ACKNOWLEDGMENTS. We thank Jianmin Liu, Xiaolun Zhang, Dhanuja Perera, Sujay Ithychanda, Esen Goksoy, Xiaoxia Wang, Koichi Fukuda, and Julia Vaynberg for technical assistance and useful discussion and Dr. Crabb for providing the mass spectrometry service. This work was supported by National Institutes of Health grants to (J.Q. and E.F.P.). R.C.P. was supported by American Heart Association postdoctoral fellowship. This work made use of the High Performance Computing Resource in the Core Facility for Advanced Research Computing at Case Western Reserve University.

1. Hynes, RO (2002) Integrins: Bidirectional, allosteric signaling machines. *Cell* 110:673–687.
2. Qin J, Vinogradova O, Plow EF (2004) Integrin bidirectional signaling: A molecular view. *PLoS Biol* 2:714–717.
3. Adair BD, Yeager M (2002) Three-dimensional model of the human platelet integrin alphaIIbbeta 3 based on electron cryomicroscopy and x-ray crystallography. *Proc Natl Acad Sci USA* 99:14059–14064.
4. Schneider D, Engelman DM (2004) Involvement of transmembrane domain interactions in signal transduction by alpha/beta integrins. *J Biol Chem* 279:9840–9846.
5. Luo BH, Springer TA, Takagi J (2004) A specific interface between integrin transmembrane helices and affinity for ligand. *PLoS Biol* 2:776–786.
6. Lau TL, Kim C, Ginsberg MH, Ulmer TS (2009) The structure of the integrin alphaIIb-beta3 transmembrane complex explains integrin transmembrane signalling. *EMBO J* 28:1351–1361.
7. Vinogradova O, et al. (2002) A structural mechanism of integrin alpha(IIb)beta(3) ''inside-out'' activation as regulated by its cytoplasmic face. *Cell* 110:587–597.
8. Weljie AM, Hwang PM, Vogel HJ (2002) Solution structures of the cytoplasmic tail complex from platelet integrin alpha IIb- and beta 3-subunits. *Proc Natl Acad Sci USA* 99:5878–5883.
9. Bhunia A, Tang XY, Mohanram H, Tan SM, Bhattacharjya S (2009) NMR solution conformations and interactions of integrin αLβ2 cytoplasmic tails. *J Biol Chem* 284:3873–3884.
10. Kim M, Carman CV, and Springer TA. (2003) Bidirectional transmembrane signaling by cytoplasmic domain separation in integrins. *Science* 301:1720–1725.
11. Partridge AW, Liu S, Kim S, Bowie JU, Ginsberg MH (2005) Transmembrane domain helix packing stabilizes integrin alphaIIbbeta3 in the low affinity state. *J Biol Chem* 280:7294–7300.
12. Luo BH, Carman CV, Takagi J, Springer TA (2005) Disrupting integrin transmembrane domain heterodimerization increases ligand binding affinity, not valency or clustering. *Proc Natl Acad Sci USA* 102:3679–3684.
13. Li W, et al. (2005) A push-pull mechanism for regulating integrin function. *Proc Natl Acad Sci USA* 102:1424–1429.
14. Kim C, Lau TL, Ulmer TS, Ginsberg MH (2009) Interactions of platelet integrin {alpha}IIb and {beta}3 transmembrane domains in mammalian cell membranes and their role in integrin activation. *Blood* 113:4747–4753.
15. Gottschalk KE (2005) A coiled-coil structure of the alphaIIbbeta3 integrin transmembrane and cytoplasmic domains in its resting state. *Structure (London)* 13:703–712.
16. Lin X, Tan SM, Law SK, Torres J (2006) Unambiguous prediction of human integrin transmembrane heterodimer interactions using only homologous sequences. *Proteins* 65:274–279.
17. Zhu J, et al. (2009) The structure of a receptor with two associating transmembrane domains on the cell surface: Integrin alphaIIbbeta3. *Mol Cell* 34:234–249.
18. Metcalf DG, Kulp DW, Bennett JS, Degrado WF (2009) Multiple approaches converge on the structure of the integrin alphaIIb/beta3 transmembrane heterodimer. *J Mol Biol* 392:1087–1101.
19. Ulmer TS, Yaspan B, Ginsberg MH, Campbell ID (2001) NMR analysis of structure and dynamics of the cytosolic tails of integrin alpha IIb beta 3 in aqueous solution. *Biochemistry* 40:7498–7508.
20. Li R, et al. (2001) Oligomerization of the integrin alpha IIbbeta 3: Roles of the transmembrane and cytoplasmic domains. *Proc Natl Acad Sci USA* 98:12462–12467.
21. Matthews EE, Zoonens M, Engelman DM (2006) Dynamic helix interactions in transmembrane signaling. *Cell* 127:447–450.
22. Zhu J, et al. (2008) Structure of a complete integrin ectodomain in a physiologic resting state and activation and deactivation by applied forces. *Mol Cell* 32:849–861.
23. Vinogradova O, et al. (2004) Membrane-mediated structural transitions at the cytoplasmic face during integrin activation. *Proc Natl Acad Sci USA* 101:4094–4099.
24. Lau TL, Dua V, Ulmer TS (2008) Structure of the integrin alphaIIb transmembrane segment. *J Biol Chem* 283:16162–16168.
25. Lau TL, Partridge AW, Ginsberg MH, Ulmer TS (2008) Structure of the integrin beta3 transmembrane segment in phospholipid bicelles and detergent micelles. *Biochemistry* 47:4008–4016.
26. Hughes, et al. (1996) Breaking the integrin hinge: A defined structural constraint regulates integrin signaling. *J BiolChem* 271:6571–6574.
27. Lupas AN, Gruber M (2005) The structure of alpha-helical coiled coils. *Adv Protein Chem* 70:37–78.
28. Blankenfeldt W, Thomä NH, Wray JS, Gautel M, Schlichting I (2006) Crystal structures of human cardiac beta-myosin II S2-Delta provide insight into the functional role of the S2 subfragment. *Proc Natl Acad Sci USA* 103:17713–17717.
29. McNamara C, et al. (2008) Coiled-coil irregularities and instabilities in group A Streptococcus M1 are required for virulence. *Science* 319:1405–1408.
30. Barry WT, et al. (2002) Molecular basis of CIB binding to the integrin alpha IIb cytoplasmic domain. *J Biol Chem* 277:28877–28883.
31. Yuan W, et al. (2006) CIB1 is an endogenous inhibitor of agonist-induced integrin alphaIIbbeta3 activation. *J Cell Biol* 172:169–175.
32. Ahrens IG, et al. (2006) Evidence for a differential functional regulation of the two beta(3) integrins alpha(V)beta(3) and alpha(IIb)beta(3). *Exp Cell Res* 312:925–937.
33. Hato T, et al. (2008) Cooperative role of the membrane-proximal and -distal residues of the integrin beta3 cytoplasmic domain in regulation of talin-mediated alpha IIb beta3 activation. *J Biol Chem* 283:5662–5668.
34. Ma YQ, et al. (2006) Regulation of integrin alpha(IIb)beta(3) activation by distinct regions of Its cytoplasmic tails. *Biochemistry* 45:6656–6662.
35. Wegener KL, et al. (2007) Structural basis of integrin activation by talin. *Cell* 128:171–182.
36. Goksoy E, et al. (2008) Structural basis for the autoinhibition of talin in regulating integrin activation. *Mol Cell* 31:124–133.
37. Shen Y, Vernon R, Baker D, Bax A (2009) De novo protein structure generation from incomplete chemical shift assignments. *J Biomol NMR* 43:63–78.
38. Sharma CP, Ezzell RM, Arnaout MA (1995) Direct interaction of filamin (ABP-280) with the beta 2-integrin subunit CD18. *J Immunol* 154:3461–3470.
39. Kiema T, et al. (2006) The molecular basis of filamin binding to integrins and competition with talin. *Mol Cell* 21:337–347.
40. Ithychanda SS, et al. (2009) Migfilin, a molecular switch in regulation of integrin activation. *J Biol Chem* 284:4713–4722.
41. Takagi J, Petre BM, Walz T, Springer TA (2002) Global conformational rearrangements in integrin extracellular domains in outside-in and inside-out signaling. *Cell* 110:599–611.